Engineering Fracture Mechanics Vol. 45, No. 3, pp. 393–398, 1993
Printed in Great Britain.

0013-7944/93 $6.00 + 0.00

FRACTURE OF ROCK: EFFECT OF LOADING RATE

ZDENĚK P. BAŽANT, SHANG-PING BAI and RAVINDRA GETTU

Center for Advanced Cement-Based Materials, Northwestern University, Evanston, IL 60208, U.S.A.

Abstract—Fracture parameters of limestone at loading rates ranging over four orders of magnitude in the static regime are determined using the size effect method. Three sizes of three-point bend notched specimens were tested under crack-mouth opening displacement control. The fracture toughness and nominal strength decrease slightly with a decrease in rate, but the fracture process zone length and the brittleness of failure are practically unaffected. The effect of material creep on the fracture of limestone is negligible in the time range studied here. However, the methodology developed for characterizing rate effects in static fracture can be easily applied to other brittle-heterogeneous materials. The decrease of fracture toughness as a function of the crack propagation velocity is described with a power law. A formula for the size- and rate-dependence of the nominal strength is also presented.

INTRODUCTION

Bond rupture is a rate process governed by Maxwell distribution of molecular thermal energies and characterized by activation energy. Therefore, fracture in all materials is rate-sensitive. This has been experimentally demonstrated for rock in the dynamic range, but not in the static range. However, knowledge of this rate effect is very important for may practical applications in mining, geotechnical engineering and geology. The present paper reports new experimental results on the static fracture of limestone at loading rates ranging over four orders of magnitude. The corresponding times to failure range from about 2 sec to almost 1 day.

EXPERIMENTAL DETAILS

All specimens were cut from the same block of Indiana (Bedford) limestone. Three sizes of three-point bend (single-edge-notched) fracture specimens (Fig. 1) were tested. The depths, d, of the beams were 25, 51 and 102 mm (1, 2 and 4 in.), and the thickness, b, of each was 13 mm (0.5 in.). The specimens were cut such that the bending plane of the rock was normal to the load. Notches of 1.3 mm (0.05 in.) width were cut with a steel saw blade. Aluminum bearing plates of length equal to half the beam depth were epoxied at the ends to provide support. The fracture tests were conducted under constant crack-mouth opening displacement (CMOD) rates in a 89 kN (20 kip) closed-loop controlled machine with a load cell operating in the 890 N (200 lb) range. The CMOD was monitored with a transducer (LVDT of 0.127 mm range) mounted across the notch. Four series of tests were performed; each series consisted of six specimens, two in each size (see Table 1). The CMOD rates were chosen so that all specimens in a series reached their peak load in about the same time, t_p. The average t_p values were 2.3, 213, 21,420 and 82,500 sec for the different series. The typical load–CMOD curves for each size are shown in Fig. 2. From the initial slopes of these curves, the initial elastic modulus E_0 of the rock was calculated, for each test, using linear elastic fracture mechanics (LEFM) formulas [1]; see Table 1.

IDENTIFICATION OF FRACTURE PARAMETERS

The size effect method [2] is used to determine the material fracture parameters from the test data. The method has previously been verified for the fracture of limestone [3], as well as other rocks and concrete [4, 5]. Recently, it has also been used in a study of the effect of loading rate on the fracture of concrete [6]. The method is based on the size effect law [7], which is:

$$\sigma_N = \frac{Bf_u}{\sqrt{(1+\beta)}}, \quad \beta = \frac{d}{d_0}, \tag{1}$$

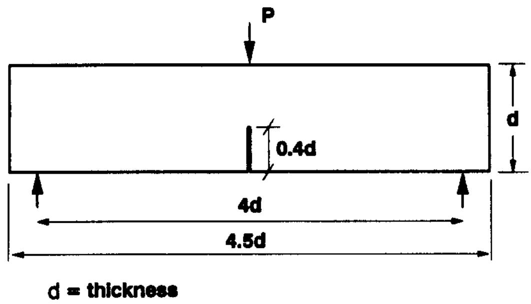

Fig. 1. Fracture specimen geometry.

where $\sigma_N = P_u/bd$ = maximum nominal stresses of geometrically similar fracture specimens, P_u = maximum load, d = characteristic dimension (chosen here as the beam depth), b = specimen thickness (constant, for two-dimensional similarity), Bf_u and d_0 = empirical parameters, and β = brittleness number. When β is very small (e.g. $\beta \ll 0.1$), σ_N is almost independent of size, as in plastic limit analysis. When β is large (e.g. $\beta \gg 10$), the size-dependence follows LEFM (i.e. $\sigma_N \propto 1/\sqrt{d}$). In the transition zone, nonlinear fracture mechanics needs to be applied.

For determining the parameters from σ_N data, eq. (1) can be transformed to $Y = AX + C$, where $X = d$ and $Y = 1/\sigma_N^2$. Then, $Bf_u = 1/\sqrt{C}$ and $d_0 = C/A$ [4]. By linear regression analysis of the data for the four series of tests, the parameters and coefficients of variation of errors, $\omega_{Y|X}$, have been computed and are listed in Table 2. The data and the fits [eq. (1)] are shown in Fig. 3. It can be seen that the size effect law represents the trend reasonably well, at all the loading rates. It is clear that the data cannot be represented by either LEFM (a straight line with a slope of $-1/2$) or strength criteria (horizontal line $\sigma_N = Bf_u$).

Using the values of Bf_u and d_0, fracture parameters can be calculated as follows [4, 5, 7]:

$$K_{Ic} = Bf_u\sqrt{(d_0 g(\alpha_0))}, \quad c_f = \frac{d_0 g(\alpha_0)}{g'(\alpha_0)}, \quad G_f = \frac{K_{Ic}^2}{E'}, \tag{2}$$

Table 1. Test data

Series	Dimensions† (mm × mm × mm)	CMOD rate (10^{-6} mm/sec)	Peak load (N)	Time to peak (sec)	E_0‡ (GPa)
	457 × 102 × 13	15,900	445	2.1	40
		15,900	472	2.2	32
Fast	229 × 51 × 13	10,600	281	2.0	35
		10,600	291	2.4	24
	114 × 25 × 13	5770	178	2.4	35
		5770	165	2.2	35
	457 × 102 × 13	159	436	176	33
		141	414	194	30
Usual	229 × 51 × 13	106	269	237	30
		106	271	210	30
	114 × 25 × 13	57.7	153	248	29
		63.5	165	215	30
	457 × 102 × 13	1.42	394	23,175	30
		1.42	383	16,875	32
Slow	229 × 51 × 13	0.978	245	26,000	28
		0.978	240	20,475	25
	114 × 25 × 13	0.706	147	15,750	32
		0.508	153	26,250	34
	457 × 102 × 13	0.353	385	81,900	27
		0.318	387	79,000	34
Very slow	229 × 51 × 13	0.236	262	87,800	32
		0.236	265	82,350	27
	114 × 25 × 13	0.160	140	72,000	26
		0.160	136	92,000	25

†Length × depth × thickness.
‡Initial modulus from load–CMOD compliance.

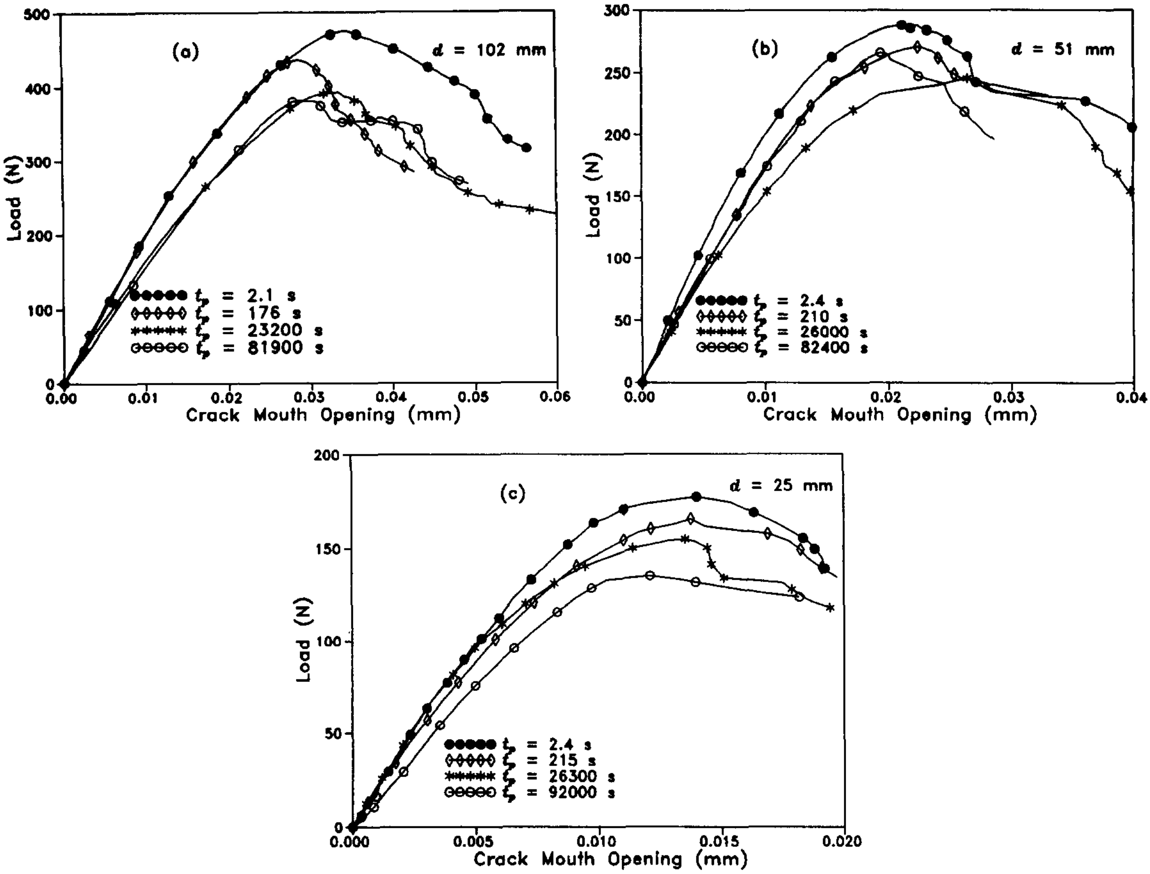

Fig. 2. Typical load–CMOD curves for each specimen size.

where K_{Ic} = fracture toughness, c_f = effective length of the fracture process zone, and G_f = fracture energy. Function $g(\alpha)$ is the non-dimensionalized energy release rate defined by the LEFM relation $G = P^2 g(\alpha)/E'b^2 d$, where G = energy release rate of the specimen, P = load, $\alpha = a/d$ = relative crack length, $g'(\alpha) = \mathrm{d}g(\alpha)/\mathrm{d}\alpha$, a = crack length, $\alpha_0 = a_0/d$, a_0 = notch length of traction-free crack length, $E' = E$ for plane stress, $E' = E/(1 - \nu^2)$ for plane strain, E = Young's modulus, and ν = Poisson's ratio. Function $g(\alpha)$ can be obtained from handbooks (e.g. [1]) or from LEFM analysis.

Fracture parameters are defined here for the limiting case of an infinitely large specimen at failure. Then, an infinite-size extrapolation of eq. (1) provides material parameters [eq. (2)] that are practically size- and shape-independent [5]. Using the values $g(\alpha_0) = 62.84$ and $g'(\alpha_0) = 347.7$ (from [1]), and assuming plane stress conditions, the fracture parameters for the four series can be computed; see Table 2, in which the average values of K_{Ic} and c_f as well as their coefficients of variation are listed. The E-value for each series is taken as the average initial modulus E_0, and is used in eq. (2) for computing G_f (see Table 2).

VARIATION OF FRACTURE PARAMETERS

The test results show that as the time to peak load, t_p, increases, the fracture toughness K_{Ic} decreases. Since the fracture energy G_f is proportional to K_{Ic}^2, its decrease with slower loading rates is even stronger. The same trends have also been observed in similar materials, such as hardened cement paste [8], concrete [6], and ceramics at high temperatures [9].

To describe the influence of loading rate, we follow several other investigators by adopting a power function of crack velocity v:

$$K_{Ic} = K_0 \left(\frac{v}{v_0} \right)^n, \tag{3}$$

Table 2. Fracture parameters

Series	Avg. t_p (sec)	Bf_u (MPa)	d_0 (mm)	$\omega_{\eta X}$	K_{Ic} Avg. (MPa$\sqrt{\text{mm}}$)	K_{Ic} ω	c_f Avg. (mm)	c_f ω	Avg. E_0 (GPa)	G_f (N/m)
Fast	2.3	0.693	36.2	0.07	33.1	0.13	6.5	0.19	33.5	32.7
Usual	213	0.645	36.3	0.07	30.8	0.12	6.6	0.19	30.3	31.3
Slow	21,400	0.614	31.9	0.04	27.5	0.08	5.8	0.12	30.2	25.0
Very slow	82,500	0.589	36.5	0.11	28.2	0.19	6.6	0.28	28.5	27.9

ω = coefficient of variation.

where K_0 is the fracture toughness corresponding to a reference velocity, v_0, chosen here as $v_0 = 0.01$ mm/sec. Since the effective (LEFM) crack tip is roughly at a distance c_f from the notch tip at the peak load, we use the approximation

$$v = c_f/t_p. \tag{4}$$

Then, by fitting the test results with eq. (3) (see Fig. 4), we obtain $n = 0.0173$ and $K_0 = 30.0\ \text{MPa}\sqrt{\text{mm}}$. Note that, alternatively, beam deflection or crack opening rates have been used instead of v in other studies.

In similar tests of concrete [6], it was found that, with an increase in time to failure, the group of data for the three sizes of specimens shifts to the right, i.e. toward the LEFM asymptote, when plotted as in Fig. 3. This implies that, for higher t_p, the process zone length c_f decreases and the brittleness of failure, characterized by β [eq. (1)], increases.

Rather interestingly, no such trend is observed from the present results of limestone. For all t_p, the data remain within the same part of the size effect curve. This is reflected by the fact that c_f is practically constant ($c_f \simeq 6$ mm; Table 2), implying that the brittleness of fracture in limestone is rate-independent within the time range studied here. This difference in the behavior (for the present load durations) from concrete may be explained by the lack of significant creep [10]. Concrete exhibits marked viscoelastic creep in the bulk of the test specimen, as well as high nonlinear creep in and near the fracture process zone.

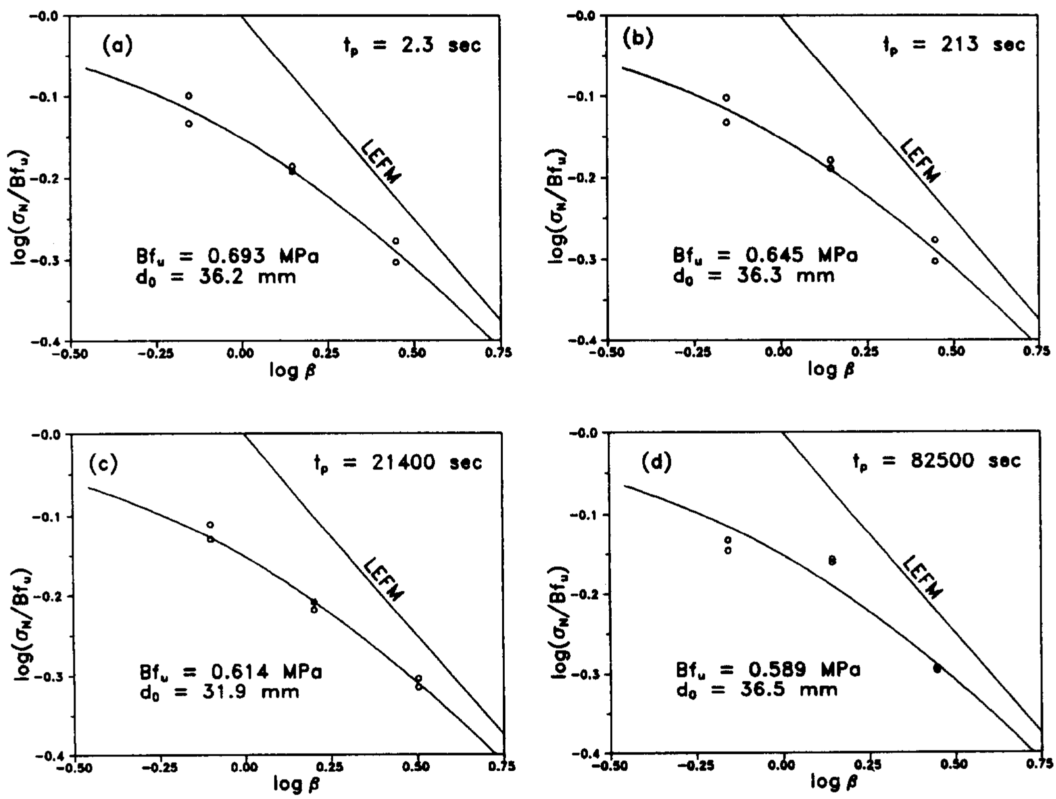

Fig. 3. Size effect curves at different times to peak load.

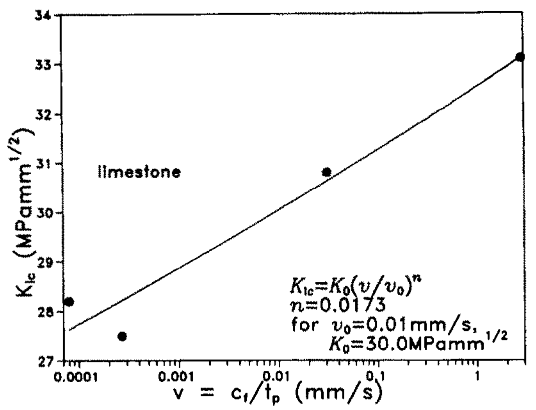

Fig. 4. Variation of fracture toughness with crack velocity.

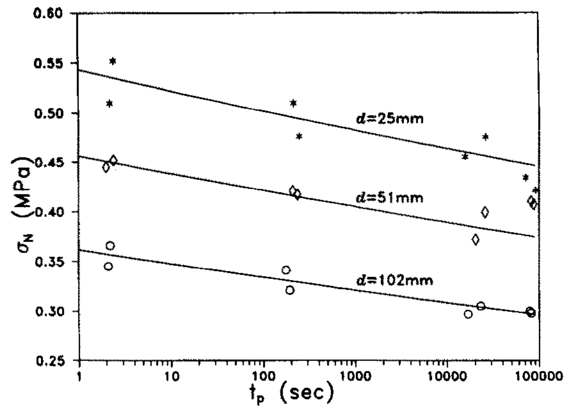

Fig. 5. Influence of specimen size and time to failure on nominal strength.

EFFECT OF RATE ON STRENGTH AND YOUNG'S MODULUS

Several investigators have demonstrated that the strength of rock generally increases with an increase in the loading rate (e.g. [11, 12]). This is also observed here from Table 1. When the loading rate slows by four orders of magnitude, the maximum nominal stress decreases by more than 16%. This phenomenon, which is similar to the change in K_{Ic}, has also been observed in other materials [13]. It may be attributed to the statistical nature of the failure of molecular bonds (particularly the activation energy theory and the Maxwell distribution of thermal energies).

The strength of a quasi-brittle heterogeneous material is generally difficult to measure objectively because of its dependence on specimen size and shape, and because failure does not occur simultaneously at all points but is progressive. However, strength (or failure stress) is correlated to the fracture toughness since failure occurs by unstable crack propagation; higher toughness implies higher resistance against failure.

Equations (1) and (2) can be combined to give the size effect on the nominal strength (maximum nominal stress) in terms of the material fracture parameters [5]:

$$\sigma_N = \frac{K_{Ic}}{\sqrt{(g'(\alpha_0)c_f + g(\alpha_0)d)}}. \tag{5}$$

Substituting for K_{Ic} from eq. (3), and c_f from eq. (4), one obtains a relation for the dependence of the nominal strength on the failure time:

$$\sigma_N = \frac{K_0}{\sqrt{(g'(\alpha_0)c_f + g(\alpha_0)d)}}\left(\frac{c_f}{v_0 t_p}\right)^n. \tag{6}$$

Since c_f is not systematically affected by the loading rate, the average value of 6.4 mm is considered. Equation (6) may then be plotted, along with the test data, for the different sizes tested (Fig. 5). The agreement is acceptable.

The test results also indicate that the average initial elastic modulus decreases slightly with an increase in the time to peak load (Table 2). Such an effect has been observed for several rocks in the dynamic range [14].

CONCLUSIONS

(1) For times to peak load ranging from 2 to 80,000 sec, the measured nominal strengths of fracture specimens of limestone agree with the size effect law.
(2) The fracture toughness and failure stress decrease with increasing failure time. However, the fracture process zone size and the brittleness of failure appear to be unaffected by the loading rate.
(3) Since there is insignificant creep outside the process zone of limestone in the time range studied, the effective process zone size does not change as the loading rate is varied.

Acknowledgements—This work was partially supported by AFOSR contract 91-0140 with Northwestern University, and the Center for Advanced Cement-Based Materials at Northwestern University (NSF Grant DMR-8808432). S. P. Bai is grateful for support from ISTIS, Taiyuen, P.R.C., during the course of this study.

REFERENCES

[1] H. Tada, P. C. Paris and G. R. Irwin, *The Stress Analysis of Cracks Handbook*, 2nd Edn. Paris Productions, St. Louis, MO (1985).
[2] RILEM TC89, Size-effect method for determining fracture energy and process zone size of concrete. *Mater. Structures* **23**, 461–465 (1990).
[3] Z. P. Bažant, R. Gettu and M. T. Kazemi, Identification of nonlinear fracture properties from size effect tests and structural analysis based on geometry-dependent *R*-curves. *Int. J. Rock Mech. Min. Sci.* **28**, 43–51 (1991); Corrigenda. **28**, 233 (1991).
[4] Z. P. Bažant and P. A. Pfeiffer, Determination of fracture energy from size effect and brittleness number. *ACI Mater. Jl* **84**, 463–480 (1987).
[5] Z. P. Bažant and M. T. Kazemi, Determination of fracture energy, process zone length and brittleness number from size effect, with application to rock and concrete. *Int. J. Fracture* **44**, 111–131 (1990).
[6] Z. P. Bažant and R. Gettu, Rate effects and load relaxation in static fracture of concrete. Rep. No. 90-3/498r, Center of Advanced Cement-Based Materials, Northwestern Univ., Evanston, IL (1990). Also *ACI Mater. Jl* **89**(5), 456–468 (1992).
[7] Z. P. Bažant, Size effect in blunt fracture: concrete, rock, metal. *J. Engng Mech.* **110**, 5128–5135 (1984).
[8] S. Mindess, Rate of loading effects on the fracture of cementitious materials, in *Application of Fracture Mechanics to Cementitious Composites* (Edited by S. P. Shah), pp. 617–638. Martinus Nijhoff, Dordrecht (1985).
[9] S. H. Knickerbocker, A. Zangvil and S. D. Brown, Displacement rate and temperature effects in fracture of a hot-pressed silicon nitride at 1100° to 1325°C. *J. Am. Ceram. Soc.* **67**, 365–368 (1984).
[10] D. Griggs, Creep of rocks. *J. Geology* **47**, 225–251 (1939).
[11] A. Kumar, The effect of stress rate and temperature on the strength of basalt and granite. *Geophysics* **33**, 501–510 (1968).
[12] S. S. Peng, A note on the fracture propagation and time-dependent behavior of rocks in uniaxial tension. *Int. J. Rock Mech. Min. Sci.* **12**, 125–127 (1975).
[13] C. C. Hsiao, Kinetic strength of solids, in *Advances in Fracture Research* (Edited by K. Salama, K. Ravi-Chandar, D. M. R. Taplin and P. Rama Rao), Volume 4, pp. 2913–2919. Pergamon Press, Oxford (1989).
[14] K. P. Chong, J. S. Harkins, M. D. Kuruppu and A. I. Leskinen, Strain rate dependent mechanical properties of Western Oil Shale, in *28th U.S. Symp. on Rock Mechanics* (Edited by I. W. Farmer, J. J. K. Daemen, C. S. Desai, C. E. Glass and S. P. Neuman), pp. 157–164. A. A. Balkema, Rotterdam (1987).

(*Received* 8 *April* 1992)